Diffusion Flames Upwardly Propagating over PMMA: Theory, Experiment and Numerical Modeling

J-L CONSALVI[1], B. PORTERIE[1], M. COUTIN[2], L. AUDOUIN[2],
C. CASSELMAN[2], A. RANGWALA[3], S.G. BUCKLEY[3] and J.L. TORERO[4]
[1] Polytech'Marseille/DME, UMR/CNRS 6595
5 rue E. Fermi
13453 Marseille Cedex 13, France
[2] Institut de Radioprotection et de Sûreté Nucléaire, DPAM, Cadarache
13108 Saint Paul lez Durance, France
[3] Department of Mechanical and Aerospace Engineering
University of California
San Diego, La Jolla, CA 92093-0411, USA
[4] BRE/Edinburgh Centre for Fire Research
The University of Edinburgh
Edinburgh, EH9 3JL, UK

ABSTRACT

A numerical model and experiments over PMMA are used to evaluate the main assumptions used in the theoretical description of a diffusion flame established in a natural boundary layer. Flow characteristics (2-D Boundary Layer) and surface thermal balance are identified as the critical assumptions to be evaluated. Comparison of experiments, numerical results, and theoretical model serve to validate the assumptions leading to the definition of a mass transfer number but establish the need to model all three-dimensional features of the flow.

KEYWORDS: diffusion flame, upward spread, mass transfer number

NOMENCLATURE

B	Mass transfer number	T_{ig}	Ignition temperature
C_p	Specific heat	x_p	Pyrolysis front
G	Average incident radiation	y_{fl}	Stand-off distance
Gr_x	Grashoff number	**Greek**	
J	Mixture fraction	ε	Emissivity
L_{fl}	Flame Length	η	Similarity variable
L_v	Heat of pyrolysis	λ	Conductivity
$\dot{m}''_p$	Fuel mass flux	**Subscript**	
Q	Losses at the fuel surface	s	Solid
Q_p	Heat of combustion per unit mass of oxygen	fl	Flame
$\dot{q}''$	Heat Flux	inc	Incident

INTRODUCTION

The two main visible geometrical characteristics of a diffusion flame are the flame length and stand-off distance. For condensed phase fuels a pyrolysis length generally complements these parameters. The flame length and stand-off distance can be carefully measured using video cameras while the pyrolysis length using thermocouples. The

FIRE SAFETY SCIENCE–PROCEEDINGS OF THE EIGHTH INTERNATIONAL SYMPOSIUM, pp. 397-408

pyrolysis and flame lengths are the time integrated outcome of the processes occurring along the burning fuel therefore are global quantities that depend on many variables. The stand-off distance is, in contrast, defined by transport in the vicinity of the reaction, and thus is mostly affected by the external supply of oxidizer and fuel transport from the surface. So, the stand-off distance represents a quantity that can be linked to the fuel in a more direct manner than the flame length. Nevertheless, the flame and pyrolysis lengths, since they are more relevant to fire growth, have been exploited extensively while the stand-off distance has not.

Theoretical formulations showing the link between the mass transfer number and the stand-off distance were developed in the 1950's. The pioneering study of Spalding [1] developed the first expression for the droplet burning-rate as a function of the mass transfer or B number. The expression proposed by Spalding has been later extended to describe the burning rate of fire flames such as pool fires [2]:

$$\dot{m}''_P = \frac{h}{C_P}\ln(1+B) \tag{1}$$

The same approach was used by Emmons [3] to provide a solution for the burning rate induced by a diffusion flame established over a liquid fuel and subject to a forced flow parallel to the surface:

$$\dot{m}''_P = (\rho_\infty U_\infty)\frac{(\eta f' - f)}{2(\mathrm{Re}.(x/L))^{1/2}} \tag{2}$$

where f is a normalized mixture fraction variable that comes from the solution of the following differential equation

$$f''' + f \cdot f'' = 0 \tag{3}$$

with the associated boundary conditions:

$$\eta = 0 \quad , \quad f' = 0 \quad , \quad \frac{f}{f''} = -\frac{B}{2} \qquad \text{where } \eta = \frac{1}{2}\left(\frac{\mathrm{Re}}{x}\right)^{1/2}\int_0^y \rho dy$$
$$\eta \to \infty \quad , \quad f' = 2$$

and where the mass transfer number as defined by Emmons [3] is as follows:

$$B = \frac{(Q_P Y_{O_2,\infty}) - Cp_\infty (T_{ig} - T_\infty)}{L_V + Q} \tag{4}$$

The term Q represents the normalized non-convective heat transfer at the surface

$$Q = \frac{\left(\dot{q}''_C + \dot{q}''_{s,r} - \dot{q}''_f\right)}{\dot{m}''_P} \tag{5}$$

$\dot{q}''_C$ represents in-depth conduction, $\dot{q}''_{s,r}$ surface re-radiation and $\dot{q}''_f$ the radiative feedback from the flame.

Pagni and Shih [4] also developed a parallel analysis for a vertical wall subject to natural and mixed convection. A series of similar analyses together with experimental validation

have been published subsequently [5,6]. Including buoyancy gives a set of normalized momentum and species equations

$$\begin{aligned} f''' + 3ff'' - 2f'^2 &= -(L_V + Q)\left[1 + (1-J)B\right] \\ J'' + 3\,\mathrm{Pr}\ f\ J' &= 0 \end{aligned} \tag{6}$$

With the associated boundary conditions

$$\eta = 0 \quad , \quad f' = 0, \quad f(0) = BJ'(0)/3\,\mathrm{Pr} \quad and \quad J = 1$$
$$\eta \to \infty \quad , \quad f' = 0 \quad and \quad J = 0$$

where the similarity variable is now $\eta = (Gr_x^{1/4} / x\sqrt{2})\int_0^y \frac{\rho}{\rho_\infty} dy$ and

$$Gr_x = \frac{gx^3(T_W - T_\infty)}{\nu_\infty{}^2 T_\infty}$$

Making a flame sheet approximation allows to solve for the stand-off distance. The pyrolysis length remains a parameter of the solution while the flame length is generally calculated by means of an integral solution [4,5]. Roberts and Quince [7] extended this analysis to show that extinction could be predicted as a function of a critical B number. Recently this concept has been revived to describe the quenching limit of micro-gravity diffusion flames [8,9] showing that a critical mass transfer number can be linked with a critical Damköhler Number and thus with an extinction limit. This extinction limit was shown to be essential in the calculation of the flame length. Finally, the heat flux from the flame to the surface appears as a function of f from the boundary conditions associated with Eqs. 5 and 6. The main assumption being that the dominant mode of heat transfer is due to convection and therefore the net radiative contribution is assumed negligible. Several studies have discussed this assumption, notable is that of Mathews and Sawyer [10] but no clear conclusion has been reached. The practical importance of this method stems in its potential use to describe co-current flame spread. Co-current flame spread can be predicted using a simplified methodology based on the method proposed by Quintiere [11] for opposed flame spread and later extended to co-current (or upwards) flame spread, as reviewed by Fernandez-Pello [12]. Many solutions have been proposed in the literature and are described in detail by Drysdale [13]. Nevertheless, direct application of the above-described methodology has failed to provide adequate results, thus flame length and heat-fluxes have been substituted by a series of appropriate correlations and empirical constants that can lead to very good results when predicting co-current flame spread [14,15]. This approach to co-current flame spread has been favored in CFD codes [16]. Only recently, attempts have been made to revisit the original analysis to explore the reasons for the lack of agreement between experiments and model [9] concluding that two independent sets of assumptions need to be verified, those of the nature of the flow and the assumptions leading to the definition of the mass transfer number. This new analysis differs from previous attempts in that it makes extensive use of stand-off distance measurements.

The theoretical analysis assumes a 2D laminar flow that conforms to boundary layer assumptions. These constraints have been shown to have significant effects on the flame length and heat release rate. Orloff *et al*. [14] showed that the flame length correlates linearly with the pyrolysis length while the flow is laminar but shows a decaying

dependency ($L_f \approx 0.625\,(\bar{x}_P)^{0.781}$) as soon as the flow becomes turbulent. Tsai and Drysdale [15] explored the effect of lateral entrainment on the flame length and energy release rate showing significant three-dimensional effects. Hirano and co-workers [17] explored the limitations of boundary layer approximations. In contrast, a study under idealized conditions showed that even when the flow problems were resolved discrepancies between predictions and experiments still existed. A claim was made that the reason for the poor correlation between experimental results and theory was the improper definition of the mass transfer number [9].

This study calculates the upward spread of a flame by means of a transient 2-D CFD code providing the evolution of the pyrolysis and flame length as well as the stand-off distance. While keeping a 2-D formulation it eliminates boundary layer and constant property assumptions. Following a similar approach to that of Lewis *et al.* [18], comparison between model predictions and a set of experiments with PMMA allows exploration of the different assumptions. Emphasis is given to the importance of three-dimensional effects. Furthermore, independent estimation of all gas phase quantities permits the numerical evaluation of all the components of the mass transfer number. This enables a detailed evaluation of the assumptions that relate to the gas phase.

METHODS

Experimental Apparatus

The experimental combustion set-up consists of a vertical sample of Poly-Methyl Methacrylate (PMMA) 40 cm in height, 1.2 cm in thickness, and 5 cm, 10 cm and 15 cm in width, mounted on an insulation board and covered with a metal plate, as illustrated in Fig. 1. The metallic cover, extending several cm on each side of the sample, allows only the front surface of the PMMA to ignite and burn. The sample is ignited at the bottom using an electrical wire. A ruled reference on the plate provides a visual indication of the extent of flame spread at a given time. Five thermocouples are fed through holes drilled from the back of the sample and melted on to the surface, and five additional thermocouples are placed on the back of the sample between the fuel and the insulation. The thermocouples are evenly spaced to provide temperature data, indicating the progression of the pyrolysis front and an estimate of the thermal thickness of the material. The sample is ignited in a ventilated enclosure with an electrically heated Kanthal wire. Two CCD cameras (720 x 576 pixels) are used to obtain a frontal and a side view of the flame. The field of view is chosen to obtain an error on the stand-off distance of less than 5%. Based on the characteristic times scales for propagation, an average of all images in a 10 second period was used to obtain an average stand-off distance and flame shape. First, each image is converted to grey levels (0-255) and then all values are averaged leading to an average image. The stand-off distance and flame length where determined establishing a threshold grey level. The threshold value was varied as apart of a sensitivity analysis showing that both stand-off distance and flame length did not vary significantly with the choice of grey level. The stand-off distance was corrected for fuel regression. This was done through measurements of the burnt samples after the test. Linear functions of time and location where established for the regression rates and added to the stand-of distance. The correction never exceeded 10% of the total value. Overall 6 replicate experiments were conducted and generally good agreement was found between runs.

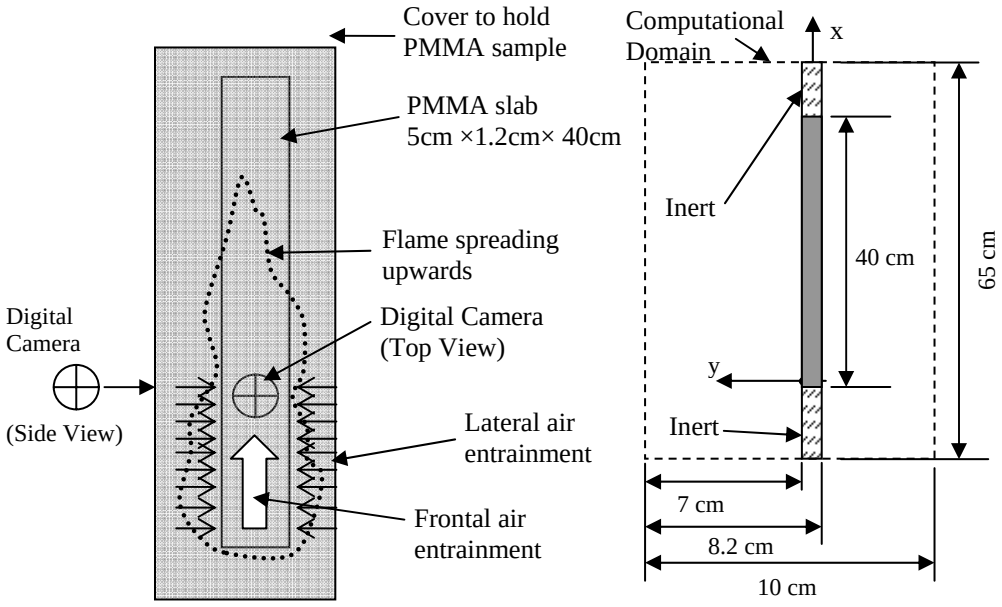

Fig. 1. Experimental set-up and computational domain.

Numerical Model

The reactive flow is computed by solving the Favre density-weighted Navier-Stokes equations in connection with the RNG k-ε turbulence model [19]. Near a solid surface, the velocity components parallel to the wall, the turbulent kinetic energy, and its rate of dissipation are treated through a local equilibrium wall log-law. The complete set of equations along with thermodynamic properties and equations of state can be found in [20].

Combustion model

In the present study, the Methyl-Methacrylate (MMA)/air reactive system is modeled as a simplified one-step chemical reaction

$$C_5H_8O_2 + 6O_2 + 22.57N_2 \rightarrow 5CO_2 + 4H_2O + 22.57N_2 \quad (7)$$

The consumption rate of fuel is calculated as the minimum of the Eddy Break-Up expression [21] (mixing-controlled regime) and an Arrhenius expression (kinetically-controlled regime) given by Wu *et al.* [22] for the MMA.

Radiation Model

In the radiation model, the grey assumption is used which implies that the absorption coefficient is independent of the wavelength of radiation. The model requires the solution of the radiative transfer equation (RTE). The absorption coefficient is calculated from the contributions from soot [23] and from the combustion products [21].

Soot formation model

To quantify soot formation, the model proposed by Moss and Stewart [24] that includes the processes of nucleation, heterogeneous surface growth and coagulation is used. This model requires the solution of two additional conservation equations for the soot mass

fraction and number density. Soot oxidation is included using the model of Naggle and Strickland-Constable [25].

Pyrolysis model

The volatilisation of PMMA is modelled as a phase change at a constant surface temperature of 630K. In the solid, the one-dimensional heat transfer equation

$$\rho_s C_{ps} \frac{\partial T}{\partial t} = \frac{\partial}{\partial x}\left(\lambda_s \frac{\partial T}{\partial x} \right) \tag{8}$$

is solved and surface regression is neglected. At the solid surface exposed to the flame the boundary conditions are as follows

- before pyrolysis:

$$-\lambda_s \frac{\partial T}{\partial x} = h\left(T_g - T\right) + \varepsilon\left(\dot{q}^{"}_{r,inc} - \sigma T^4\right) \tag{9}$$

- after pyrolysis:

$$T = T_{ig}$$
$$-\lambda_s \frac{\partial T}{\partial x} + \dot{m}^{"}_p L_v = h\left(T_g - T\right) + \varepsilon\left(\dot{q}^{"}_{r,inc} - \sigma T^4\right) \tag{10}$$

At the rear surface of the slab, the boundary condition is:

$$\lambda_s \frac{\partial T}{\partial x} = h\left(T - T_a\right) + \varepsilon\left(\dot{q}^{"}_{r,inc} - T_a{}^4\right) \tag{11}$$

The incident radiative flux, $\dot{q}^{"}_{r,inc}$, is computed from the radiation model.

Numerical Procedure

The conservation equations are discretized on a staggered, non-uniform Cartesian grid by a finite-volume procedure with a second-order backward Euler scheme for time integration. Diffusion terms are approximated from a second-order central difference scheme. For the convective terms, the ULTRASHARP approach [26] is used. The pressure-velocity linked equations are solved using the Iterative PISO algorithm [27]. The RTE is solved using the FVM with a 2x16 angular mesh [28]. The heat and mass transfer conjugated problem at the gas solid interface is treated through a blocked-off region procedure [20].

Computational Details

The model is applied to a two-dimensional configuration. The physical problem involves a 10 cm x 65 cm domain. A 1.2 cm x 40 cm PMMA slab is located at 7 cm from the west boundary (Fig. 1). A non-uniform mesh with 43x250 cells is used and the time step is 0.025s. The origin of the coordinate axis is the bottom exposed corner of the PMMA slab. Ignition is produced by means of a radiative heat flux applied between 0< x <0.2 cm. The ignition flux is eliminated immediately after the onset of the combustion reaction. Time zero is defined as the instant when the fuel surface attains the pyrolysis temperature. The values of the pyrolysis model parameters adopted in this study are: ρ_s =1200 kg/m^3 [29], λ =0.1874W/m^2/K [29], C_p=2100J /kg/K [4], L_v= 2.7 10^6 J/kg [30], ε=0.927 and T_p=630K [29].

RESULTS AND DISCUSSIONS

Flames were allowed to propagate upwards and the flame and pyrolysis lengths were recorded. The pyrolyis length was extracted from the thermocouple histories and defined as the location where the thermocouple reached 630 K [9]. Figure 2 presents the evolution of these variables with time. All length scales are normalized by the plate length (L_{plate}) and times by the characteristic residence time ($\tau_c = L_{plate}/U_B$ *with* $U_B = \sqrt{g(T_{ig} - T_\infty)L_{plate}/T_\infty}$). To avoid crowding of the figure only data for 5 cm and 15 cm width is presented.

The flame length shows a linear dependency with time. This tendency is well reproduced by the numerical model. The width of the sample seems to have no effect on this variable. The evolution of the pyrolysis length seems to follow a similar trend initially but eventually the wider sample accelerates. The numerical model seems to follow this trend in a more precise manner. These observations seem to evidence some three-dimensional effects unaccounted by the 2-D model. Figure 2c compares the current results with experiments from the literature. In all cases some level of confinement is present in the results of references [14,31,32]. The data from the literature is consistent among different studies and shows a more pronounced accelerating trend than the current experiments. It is important to note that none of these experiments were conducted under the same conditions as the current tests, nevertheless the comparison serves to highlight the importance of the flow assumptions. Orloff [14] uses a 157 cm high, 4.5 cm thick and 41 cm wide PMMA sample with water-cooled sidewalls. Given the larger width it is expected to see a more pronounced accelerating trend. It is important to reiterate that for these experiments lateral entrainment was precluded by side walls. Saito [32] uses a 30 cm wide sample with wire mesh side screens placed at 75 cm from the sample. Given that the width of the sample is smaller, it will be expected for the pyrolysis length to increase at a rate bounded by the 15 cm and 41 cm samples; nevertheless, this data shows a more pronounced acceleration. In this case there is no lateral confinement. Tewarson et [31] uses a 10 cm wide 2.5 cm thick and 30-60 cm in height PMMA sample with a co-flow of 0.09 m/s was used. The co-flow is intended to reduce 3-D effects. These results clearly show that the exact nature of the flow determines the rate at which the flame spreads. Furthermore, it indicates that side entrainment accelerates or decelerates the propagation rate and that the width of the sample represents a relevant length scale for this buoyantly induced flow. Side entrainment affects spread but does not seem to affect the evolution of the flame height. This could be due to a simultaneous increase in the oxidizer supply, thus a reduction of the flame length.

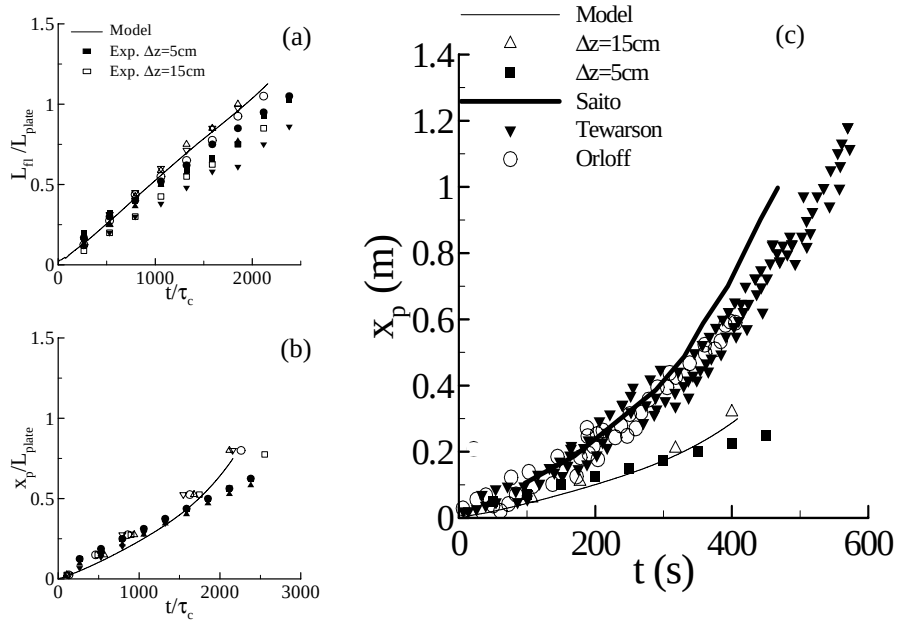

Fig. 2. Characteristic length scales as a function of time, comparison of model and experiments: (a) flame length (b) pyrolysis length, and (c) comparison of current data with other experiments in the literature: Tewarson [31], Orloff [14], and Saito [32].

Pyrolysis and flame length show that a 2-D representation of this problem might not be sufficient. The stand-off distance is therefore defined numerically and experimentally. As indicated in Fig. 3b the flame evidences an abrupt transition between the visible yellow zone and a weaker blue region. The transition indicates the completion of the soot oxidation process (absence of soot). Any soot in the proximity of the flame will glow, thus the absence of yellow glow indicates the absence of soot. Figure 3a shows two representative cross sections of the soot volume fraction and the temperature. It can be clearly seen that the complete consumption of soot coincides with the peak temperature. Therefore, numerically, the stand-off distance will be defined as the location of the peak temperature.

The stand-off distance (y_{fl}) is presented in Fig. 4 at two different instants. The results are compared with the numerical formulation and with the theoretical solution as defined by Pagni and Shih [4]: $y_{fl} = \frac{\sqrt{2}x}{Gr_x^{1/4}} \int_0^{\eta_{fl}} \frac{\rho_\infty}{\rho} d\eta$. The stand-off distance is non-dimensionalized by a characteristic boundary layer thickness ($\delta_c = L_{plate} \Big/ \sqrt{U_B L_{plate} / \nu_\infty}$). The solution to the stand-off distance requires a B number. Values in the literature range from 1 to approximately 3 [4,10], therefore the theoretical stand-off distance was evaluated for three representative values within this range.

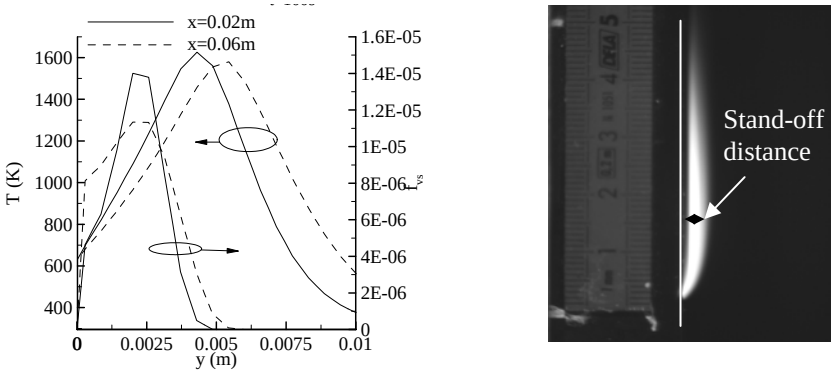

(a) (b)

Fig. 3. (a) Temperature and soot volume fraction as a function of the distance to the wall for x=0.02m and x=0.06m at t=210s. (b) Experimental measure of the stand-off distance.

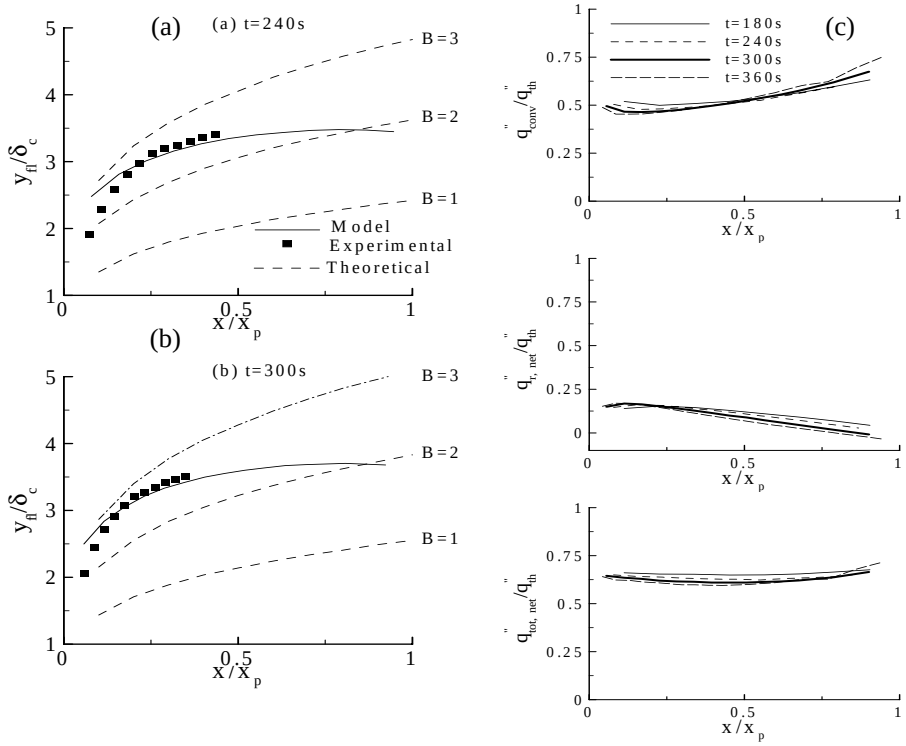

(c)

Fig. 4. (a) and (b) Dimensionless stand-off distance as a function of the dimensionless distance from the flame leading edge, (c) Dimensionless convective flux, net radiative flux and net total flux as a function of the dimensionless distance from the flame leading edge.

The experimental results show discrepancies with the theoretical model, independent of the value of B. In contrast, the numerical solution seems to reproduce well the stand-off distance. Close to the leading edge, there is disagreement between the numerical formulation and the experimental results. This could be due to three potential sources of error: increased experimental error at the leading edge, separation of the flow, which is difficult to model numerically, or the influence of the artificial numerical ignition.

The above results clearly show that the numerical solution captures the features of the flame geometry in a more precise manner. This could be attributed to a better prediction of the flow field. In addition, the numerical model solves the energy balance at the surface to obtain the burning rate (Eq. 10), thus the discrepancy could be related to an improper definition of the mass transfer. Torero *et al*. [9] evaluated the mass transfer number for micro-gravity diffusion flames by comparing experimental and theoretical stand-off distances. These flames corresponded to a forced flow, thus followed the forced flow analysis [3,4]. The comparison showed an evolving mass transfer number controlled by the different losses (Q in Eq. 5). This observation is of great practical importance because it suggests that an empirically evaluated mass transfer number could be used to accurately apply the present model to the prediction of upward flame spread.

To clarify the role of the different components of this analysis it is important to use the numerical formulation to evaluate the main assumption behind the definition of the mass transfer number. The scaling leading to the definition of the mass transfer number requires that heat transfer is to be dominated by convection. The numerical formulation can provide all heat transfer components. The results are presented in Fig. 4c. The results are normalized by the theoretical convective heat flux at the surface: $\dot{q}''_{th} = -\frac{\lambda}{C_p} BL_v J'(0) \frac{Gr_x^{1/4}}{\sqrt{2}x} \frac{T_\infty}{T_w}$. The value for the B number used is that that produces the best match between theoretical and numerical predictions of the stand-off distance. Figure 4c shows that the magnitude of the net heat-flux is consistent between theory and numerical model. It also shows that the net radiative exchange is decreases away from the leading edge to negligible values verifying the original assumption by Emmons [3]. There is a 30% discrepancy between the net heat flux evaluated numerically and the theoretical prediction, this corresponds to in-depth heat conduction through the PMMA sample.

CONCLUSIONS

A combination of a numerical model, experimental results, and a theoretical formulation has been used to describe the stand-off distance, flame and pyrolysis lengths in an upwardly propagating flame. The results verify the main thermal assumptions leading to the definition of a mass transfer number but indicate that three-dimensional effects have a significant effect on the flame geometry. A three-dimensional formulation of the flow is therefore necessary to describe the behavior of an upward spreading flame.

Acknowledgements: The funding for J.L. Consalvi and B. Porterie was provided by IRSN while funding for A. Rangwala, S.G. Buckley, and J.L. Torero was provided by NASA Fire Safety Program of the Bioastronautics Initiative, grant # NAG-32568.

REFERENCES

[1] Spalding, D.B., “The Combustion of Liquid Fuel,” *Fuel,* 30:6-121 (1951).

[2] Spalding, D.B., *Some Fundamentals of Combustion*, Butterworths, London, 1955.

[3] Emmons , H.W., "The Film Combustion of Liquid Fuel," *Zeitschrift fur Angewande Mathematik und Mechanik,* 36:60-71 (1956).

[4] Pagni, P.J. and Shih, T.M., "Excess Pyrolyzate," *Proceedings of the 16th International Symposium on Combustion*, The Combustion Institute, 1978, pp. 1329-1343.

[5] Annamalai, K. and Sibulkin, M., "Flame Spread over Combustible Surfaces for Laminar Flow Systems, Part I: Excess Fuel and Heat Flux," *Combustion Science and Technology* 19:167-183 (1979).

[6] Kosdon, F.J., Williams, F.A., and Buman, C., "Combustion of Vertical Cellulosic Cylinders in Air," *Proceedings of the 12th International Symposium on Combustion,* The Combustion Institute, 1968, pp. 253-264.

[7] Roberts, A.F. and Quince, B.W., "A Limiting Condition for the Burning of Flammable Liquids," *Combustion and Flame,* 20:245-251 (1973).

[8] Yang, C.T. and T'ien, J.S., "Numerical Simulation of Combustion and Extinction of a Solid Cylinder in Low-Speed Cross Flow," *Journal of Heat Transfer,* 120:1055-1063 (1998).

[9] Torero, J.L., Vietoris, T., Legros, G., and Joulain, P., "Estimation of a Total Mass transfer Number from the Stand-off Distance of a Spreading Flame," *Combustion Science and Technology,* 174:187-203 (2002).

[10] Mathews, R.D. and Sawyer, R.F., "Limiting Oxygen in Index Measurement and Interpretation in an Opposed Flow Diffusion Apparatus," *Journal of Fire and Flammability,* 7:200-216 (1976).

[11] Quintiere, J.G., "A Simplified Theory for Generalizing Results from a Radiant Planel Rate of Flame Spread Apparatus," *Fire and Materials,* 5 (2) (1981).

[12] Fernandez-Pello, A.C., "The Solid Phase," *Combustion Fundamentals of Fire*, Cox J. (Ed.), Academic Press, 1995.

[13] Drysdale, D.D., *Introduction to Fire Dynamics*, John Wiley and Sons, 2nd Edition, 1999.

[14] Orloff, L., De Ris, J., and Markstein, G.H., "Upward Turbulent Fire Spread and Burning of Fuel Surface," *Proceedings of the 15th International Symposium on Combustion,* The Combustion Institute, 1974, pp 183-192.

[15] Tsai, K.G. and Drysdale, D.D., "Modelling the Early Stages of Upward Flame Spread," *Interflam 2001*, pp. 707-718, Edinburgh, UK, 2001.

[16] McGrattan, K.B., Baum, H.R., Rehm, R.G., Hamins, A., Forney, G.P., and Floy, J.E., Fire Dynamics Simulator – Technical Reference Guide (Version 2), 2001.

[17] Hirano, T., Iwai, K., and Kanno, Y., "Measurement of the Velocity Distribution in the Boundary Layer over a Flat Plate with a Diffusion Flame," *Acta Astronautic,* 17:811-818 (1972).

[18] Lewis, M.J., Rubini, P.A., and Moss, J.B., "Field Modelling of Non-Charring Flame Spread," *Proceedings of the 6th International. Symposium on Fire Safety Science*, 1999, pp. 683-694.

[19] Yakhot, V. and Orszag, S., "Renormalization Group Analysis of Turbulence," *Journal of Scientific Computing*, 1:3-51 (1986).

[20] Consalvi, J.L., Porterie, B., and Loraud, J.C., "A Blocked-off Region Strategy to Compute Fire Spread Scenarios Involving Internal Flammable Target," *Numerical Heat transfer, Part B*, to appear, 2004.

[21] Magnussen, B.F. and Hjertager, B.H., "On Mathematical Modeling of Turbulent Combustion with Special Emphasis on Soot Formation and Combustion," *Proceedings of the 16th International Symposium on Combustion*, The Combustion Institute, 1976, pp. 719-729.

[22] Wu, K.K., Fan, W.F., Chen, C.H., Liou, T.M., and Pan, I.J., "Downward Flame Spread over a Thick PMMA Slab in an opposed Flow Environment: Experiment and Modelling," *Combustion and Flame*, 132:697-707 (2003).

[23] Kent, J.H. and Honnery, D.R., "A Soot Formation Rate Map for a Laminar Ethylene Diffusion Flame," *Combustion and Flame*, 79:287-298 (1990).

[24] Moss, J.B. and Stewart, C.D., "Flamelet-based Smoke Properties for Field Modelling of Fires," *Fire Safety Journal*, 30:229-250 (1998).

[25] Nagle, J. and Strickland-Constable, R.F., "Oxidation of Carbon between 1000-2000°C," *Proceedings of the 5th Carbon Conference*, 1962, pp. 154-164.

[26] Leonard, B.P. and Drummond, J.E., "Why You Should Not Use Hybrid, Power-Law or Related Exponential Schemes for Convective Modelling. There Are Much Better Alternatives," *International Journal for Numerical Methods in Fluids* 20:421-442 (1995).

[27] Chow, W.K. and Cheung, Y.L. "Selection of Differencing Scheme on Simulating the Sprinkler Hot-Air Layer Problem," *Numerical Heat Transfer, Part A* 35:311-330 (1999).

[28] Raithby, G.D. and Chui, E.H., "A Finite Volume Method for Predicting a Radiant Heat Transfer in Enclosures with Participating Media," *Journal of Heat Transfer*, 112:415-423 (1990).

[29] Vallot E. and Coutin, M., "Etude pour l'Evolution de la Puissance du Feu – Rapport de Fin d'Etude," Note technique DPAM/SEMIC 2004/27, IRSN, 2004.

[30] Quintiere, J.G. and Rhodes, B., "Fire Growth Models for Materials," NIST-GCR-94-647, 1994.

[31] Tewarson, A. and Ogden, S.D., "Fire Behavior of PolyMethylMethacrylate," *Combustion and Flame*, 89:237-259 (1992).

[32] Saito, K., Quintiere, J.G., and Williams, F.A., "Upward Turbulent Flame Spread," *Proceedings of the 1st International Symposium on Fire Safety Science*, 1985.